Thermo-fluid dynamic performance of a ventilated pitched roof: Numerical modelling and experimental validation

Roberta Moschetti*, Alessandro Nocente, Stig Geving, Lars Gullbrekken
SINTEF AS, Department of Architecture, Materials and Structures, Trondheim, Norway
* corresponding author: roberta.moschetti@sintef.no

Abstract

Wooden ventilated pitched roofs represent a widely spread construction solution in Nordic countries. They have several benefits, including the drainage of excessive moisture from the construction and the reduction of the surface temperature to prevent snow melting and thus icing at the eaves and gutters. Modelling ventilated components is complex and requires a thorough understanding of the phenomena occurring in the air cavity, where convection plays a central role in the heat transfer process. The approach and the assumptions adopted for the roof model are therefore crucial to investigate the thermo-fluid dynamics in the air cavity. A literature review showed the need for comprehensive numerical and experimental research focusing on ventilated roof constructions, especially for Nordic climates. This article presents the thermo-fluid dynamic modelling of a ventilated pitched roof, which belongs to a full-scale experimental building located in Trondheim (Norway), the ZEB Test Cell Laboratory. A model of the roof was created using the finite element method-based software COMSOL Multiphysics. Transient simulations were performed in different climate conditions and the results of temperature and air flow speed along the cross section of the roof were compared with measurement data for validation. The simulation results show a good agreement with measurement data for both air speed and temperature in the air cavity, particularly in the summer day. The deviations in the numerical results will be object of study in future research, where the modelling approach will be further explored by testing different inputs, including boundary conditions and turbulence models.

Introduction

Buildings are worldwide responsible for significant energy use and related greenhouse gas (GHG) emissions. Therefore, the design of high-performing building envelopes is acknowledged as a key strategy for reducing energy use and GHG emissions, by also targeting cost effectiveness and indoor environmental comfort (William et al. (2021)). Among energy efficient envelope solutions, ventilated roofs are increasingly used in a variety of building categories, climates, and designs, both in renovation and new building projects. Several studies focused on the potential for cooling load savings through the use of ventilated roofs in hot climates (Gagliano et al. (2012)), but the behaviour of these roofs in cold climates was also object of investigation (Blom (2001); Bunkholt Schjøth et al. (2020)). In Nordic countries, wooden ventilated pitched roofs represent a widely employed solution and are often designed to withstand extreme weather conditions. This roof typology also offers other benefits, allowing the drainage of excessive moisture from the construction to avoid mould growth and keeping the roof temperature low enough to prevent snow melting and thus icing at the eaves and gutters (Gullbrekken et al. (2018)). The thermo-fluid dynamic performance of ventilated roofs is characterized by the phenomena occurring in the air cavity, where natural convection plays a central role in the heat transfer process. Natural ventilation within the air cavity is driven by buoyancy and wind, where the former is a result of the temperature difference between the bottom and the top of the air cavity height, while the latter is a consequence of the pressure difference between inlet and outlet related to wind forces (Lee et al. (2009)). In case of eaves-to-eaves ventilated cavities with no opening in the roof ridge, the wind influence might be dominant and the thermal buoyancy might be particularly affected by the temperatures of the roof surfaces facing different cardinal directions. Several parameters are involved in the thermal and fluid dynamics of ventilated roofs, including materials' thermo-physical properties, system geometry, and climate parameters (e.g., solar radiation, air temperature, wind speed, and wind direction). Many experimental studies were performed on ventilated roofs to measure different variables, as for instance velocity and temperature of the airflow (Nusser and Teibinger (2013); Tong and Li (2014)), but also local pressure loss coefficient (Gullbrekken et al. (2018)). The thermo-fluid dynamic performance of such complex systems was also numerically investigated through different approaches, including simplified mathematical models, as by Ciampi et al. (2005), and Computational Fluid Dynamic (CFD), as in the work of Li et al. (2016). CFD analyses are often performed with a finite volume or with a finite element method (FEM) approach, which allow an accurate prediction of the main

variables of the airflow in the ventilation cavity, using different turbulence models. However, simplifications are often adopted as CFD studies can require significant computational time, depending on the complexity of the model. For instance, the air in the roof cavity can be modelled as laminar instead of turbulent flow, as done by Säwén et al. (2021) who found a good agreement between the numerical and experimental results. Furthermore, the choice of the driving forces in the ventilated cavity represents a key factor in the modelling approach. Many studies focused, for instance, primarily on the effect of thermal buoyancy in ventilated air cavities, such as Villi et al. (2009) and Säwén et al. (2021) , while others, like Nore et al. (2010), only examined the wind influence. The review of the state-of-the-art, carried out in this study, emphasised the need for comprehensive numerical and experimental research on ventilated roofs in Nordic climates, where both buoyancy and wind effects are considered.
The aim of this paper is to illustrate the definition and validation of the thermo-fluid dynamics model of a ventilated wooden pitched roof located in Norway. The numerical model was created and then validated by comparing simulation results to measurement data available for the studied roof component.

Methods

Experimental study of the roof of the Test Cell Laboratory

The roof analysed in this article belongs to a full-scale experimental laboratory building, the ZEB Test Cell Laboratory (Figure 1), located in Trondheim, Norway (Goia et al. (2017)). The roof has a wooden structure with 40° pitch and an eaves-to-eaves ventilated air cavity, which is 552 mm wide, 48 mm high, and 10 m long. Both the lower and the upper surface of the ventilation gap consist of an oriented strand board (OSB) board, which is covered by a bitumen-based roofing membrane on the exterior exposed side, as shown in Figure 2. The roof is ventilated from eaves to eaves and there is no opening in its ridge; therefore, the ventilation in the air cavity is supposed to be mostly influenced by the wind. The roof is instrumented with sensors that monitor temperature and humidity in the air cavity, specifically on the lower surface, on the upper surface, and in the middle, where also the airflow speed is measured (see Figure 2). Eighty-one thermocouples are placed evenly in nine parallel air cavities; specifically, in each air cavity three thermocouples are placed 0.5 m above the eaves, three lay between eaves and ridge, and three are located 0.5 m below the ridge. Furthermore, air pressure devices and omnidirectional remote air velocity probes are installed in two of the air cavities. The accuracy and the measurement range of the sensors in the roof are: ± 0.10°C and -20 °C – 60 °C for the thermocouples, and $\pm 3\%$ and 0.055 m/s for the air velocity probes. A weather station is located 1.5 m above the ridge of the roof, at 10 m above ground level. Outdoor temperature, wind exposure, and global horizontal irradiance are recorded at one-minute intervals. The influence of the local weather conditions on air speed and temperature in the examined roof was previously assessed by Bunkholt Schjøth et al. (2020) and Gullbrekken et al. (2017), who collected and analysed several measurement data.

Figure 1: Photo of the Test Cell Laboratory.

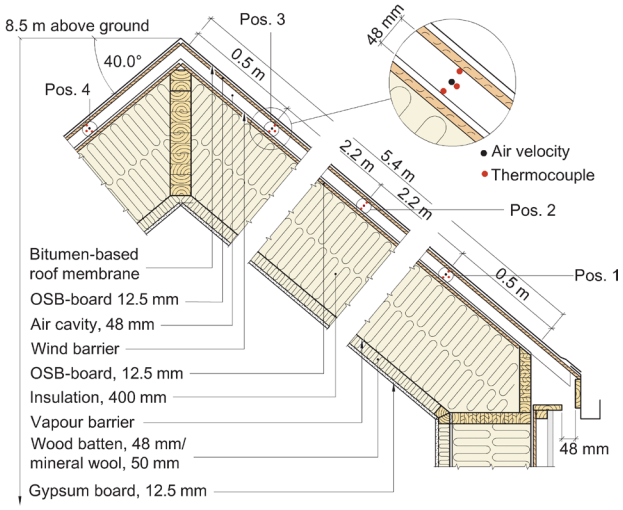

Figure 2: The Test Cell Laboratory roof. Pos. 1-4 indicate the positions of the sensors in the air cavity. Note that pos. 5 and pos. 6, which are not drawn in the figure, are located specularly to pos. 2 and pos. 1, respectively.

Numerical modelling of the roof of the Test Cell Laboratory

The roof of the ZEB Test Cell laboratory was modelled through COMSOL Multiphysics, a FEM-based software (AB (2022)). Only the ventilated cavity and the two adjacent main layers were exemplified in the geometrical model, which also includes a detailed representation of the inlet and outlet edges and a portion of the outside air. The latter allowed to consider the discharge effects at inlet and outlet, as suggested by Villi et al. (2009). Note that a reduction of ca. 20% was applied to the wideness of the air cavity's inlet/outlet, to consider the presence of an insect/bird net. The roof was modelled in two dimensions to reduce the computational time. A user-controlled mesh was defined, based on the "extra fine" coarseness setting and calibrated for Fluid Dynamics. This resulted in a free

triangular mesh for most of the domain, with border refinement for the boundary layer of the air cavity, as shown in Figure 3.

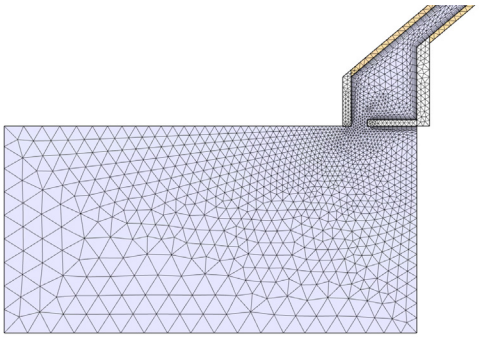

Figure 3: Detail of the mesh of the model in COMSOL Multiphysics.

In COMSOL Multiphysics, the heat transfer in solids and fluids model was coupled with the surface-to-surface radiation and the non-isothermal air flow models. This approach allowed to simulate the natural convection within the air cavity by considering the effect of both wind and thermal buoyancy.
The main thermo-physical properties of the modelled materials are illustrated in Table 1.

Table 1: Thermo-physical features of the materials used in COMSOL model.

Layer	Density, kg/m^3	Thermal conductivity, W/(m K)	Heat capacity, J/(kg K)
Air	f (P[a];T[b])	f(T)	f(T)
OSB	646	f(RH[c])	1500

[a] P is the absolute pressure

[b] T is the temperature

[c] RH is the relative humidity

The air was modelled as a weakly compressible flow, i.e. the fluid properties are functions of the temperature, but the density is evaluated at the reference absolute pressure. The turbulence model k-ε realizable was used in COMSOL Multiphysics, which solves the continuity equation for the conservation of mass (Eq. 1) and the Reynolds-averaged Navier–Stokes (RANS) equations for conservation of momentum (Eq. 2).

$$\frac{\partial \rho}{\partial t} + \rho \boldsymbol{u} \nabla \boldsymbol{u} = 0 \tag{1}$$

$$\rho \frac{\partial \boldsymbol{u}}{\partial t} + \rho \boldsymbol{u} \nabla \boldsymbol{u} = -\nabla p + \nabla(\mu(\nabla \boldsymbol{u} + (\nabla \boldsymbol{u})^T + -\frac{2}{3}\mu(\nabla \boldsymbol{u})\boldsymbol{I}) + \boldsymbol{F} \tag{2}$$

Where: ρ is the density (kg/m^3); $\boldsymbol{u}$ is the fluid velocity (m/s); p is the pressure (Pa); μ is the fluid dynamic viscosity (N s/m^2); $\boldsymbol{F}$ is an external volume force applied to the fluid, such as gravity (N/m^3); $\boldsymbol{I}$ is the velocity gradient tensor; and T represents the transpose operator.
The boundary conditions used for the turbulent flow were:

- Inlet placed on a side of one external air volume with assigned pressure conditions, as shown in Figure 4.
- Outlet placed on one side of a second external air volume with assigned pressure conditions, as shown in Figure 4.
- Acceleration of gravity vector included in the model.
- Slip condition for all walls of the outdoor environment domain other than inlet/outlet. This means no viscous effects at the wall and hence no development of boundary layers.
- No-slip conditions used to model all solid walls adjacent to the modelled airflow. This means a fluid velocity relative to the wall equal to zero.

Pressure values were given at the inlet and outlet as done by Säwén et al. (2021); however, in our study, the pressures were given in form of wind pressure coefficients (C_P), as shown in Eq. 3 and Eq. 4.

$$P_\mathrm{In} = C_\mathrm{P1} P_\mathrm{d} + P_0 \tag{3}$$

$$P_\mathrm{Out} = C_\mathrm{P2} P_\mathrm{d} + P_0 \tag{4}$$

Where: P_In is the pressure at the inlet (Pa); P_Out is the pressure at the outlet (Pa); C_P1 and C_P2 are the wind pressure coefficients (-); P_d is the dynamic pressure (Pa) at 10 m height, which is expressed as $\rho\ u^2/2$; u is the wind speed at 10 m height (m/s); ρ is the air density (kg/m^3); P_0 is the static reference pressure at 10 m height (Pa).
The C_P coefficients, used to define the pressure at the inlet and the outlet, were given as input in the weather file provided for each simulation step. Their values were calculated based on the research results presented by Gullbrekken et al. (2018) for a comparable building placed in a location in the surroundings of the Test Cell Laboratory. The discrete results of Gullbrekken et al. (2018) were interpolated through a 6^{th} degree polynomial fitting curve. The equation of the curve was then used to calculate the C_P at both inlet and outlet, for each line of the weather file, based on wind speed and direction.
Furthermore, for the turbulent flow model, the initial values of the velocity field and the relative pressure were set equal to 0 m/s and 0 Pa, respectively. Figure 4 illustrates the main boundary conditions used in the model created in COMSOL Multiphysics.

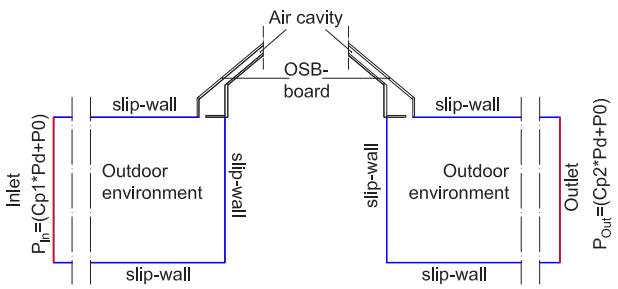

Figure 4: Boundary conditions for the model in COMSOL Multiphysiscs.

The heat and transfer in solids and fluid model used in

COMSOL Multiphysiscs is based on Eq. 5 and Eq. 6.

$$\rho C_p \frac{\partial T}{\partial t} + \rho C_p u \nabla T + \nabla q = Q + Q_{\text{ted}} \quad (5)$$

$$q = -k\nabla T \quad (6)$$

Where: ρ is the density (kg/m^3); C_p is the specific heat capacity (J/(kg·K)); T is the absolute temperature (K); u is the velocity vector (m/s); q is the heat flux by conduction (W/m^2); Q represents additional heat sources (W/m^3); Q_{ted} is the thermoelastic damping (W/m^3).
The boundary conditions used in the heat transfer in solids and fluids model were:

- Convective heat flux on the OSB-board surface towards the outdoor environment, with wind-based external convection;
- Convective heat flux on the OSB-board surface towards the indoor environment, with a user-defined heat transfer coefficient of 0.09 W/m^2/K and a constant indoor temperature of 18 °C.

For the heat transfer in solid and fluids model, the initial value of the temperature was set equal to the outdoor temperature.
Lastly, the surface-to-surface radiation model was used in COMSOL Multiphysics to characterize heat transfer by radiation with the hemicube method. In this model, a radiative heat source, q, is added to the heat transfer equation on boundaries (Eq. 7) and the radiosity, J, resulting from the sum of diffusely reflected and emitted radiation, is defined as in Eq. 8 for diffuse-gray surfaces.

$$q = (1 - \rho_\text{s})G - J \quad (7)$$

$$J = \varepsilon e_b(T) FEP(T) + \rho_\text{d} G \quad (8)$$

Where: q is the radiative heat source (W/m^2); J is the radiosity (W/m^2); ε is the surface emissivity (-); e_b (T) is the blackbody hemispherical total emissive power (W/m^2); T is the surface temperature (K); FEP is the fractional emissive power (-); ρ_s is the surface specular reflectivity (-); ρ_d is the surface diffuse reflectivity (-); G is the solar irradiation (W/m^2).
The boundary conditions for the surface-to-surface radiation model were:

- Surface of the OSB-board towards the outdoor environment modelled as diffuse with emission factor of 0.9, corresponding to bitumen-based roofing membrane;
- Surfaces of the OSB-boards towards the air cavity modelled as diffuse with emission factor of 0.85. Note that the overlying wind barrier was not modelled in COMSOL and was assumed to have the same emissivity factor as the OSB-board;
- External radiation source representing the sun, with a to-dimensional incident radiation based on the varying sun position.

Hourly climate files were created from data collected from the weather station placed on the Test Cell Laboratory roof. Transient simulations were run for a 6-hours period and a 1-minute time step, in two main days, i.e. a hot summer day with relatively high solar radiation and temperature, but low wind speed (31^{st} of August in 2019); a cold winter day with low temperature and solar radiation, but high wind speed (10^{th} of December in 2019).
Figure 5 and Figure 6 illustrate the outdoor temperature and wind speed trends during the simulated periods on the 31^{st} of August and the 10^{th} of December.

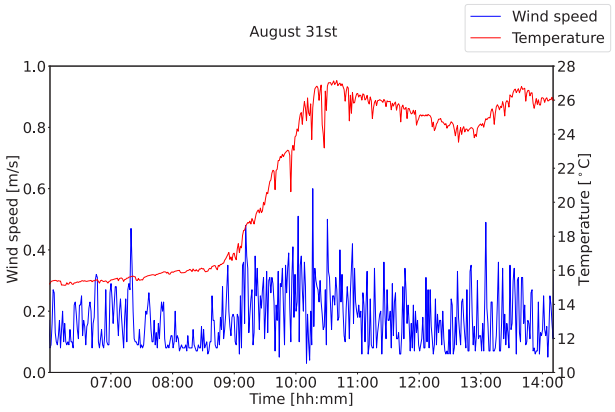

Figure 5: Wind speed and outdoor temperature measured by the weather station on the 31^{st} of August.

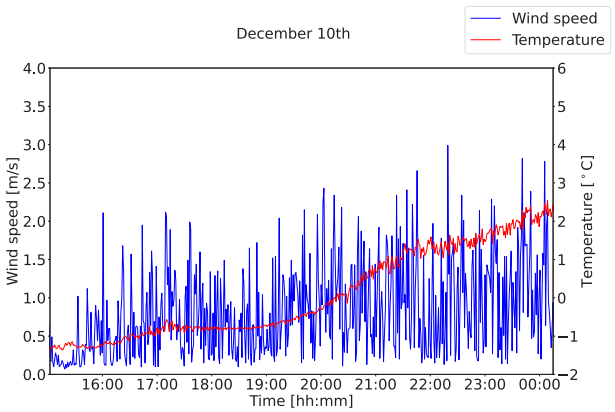

Figure 6: Wind speed and outdoor temperature measured by the weather station on the 10^{th} of December.

As the climatic data vary significantly over time, an Helmholtz filter was used in COMSOL Multiphysics (Lazarov and Sigmund (2011)). This allowed to smoothen the data series and avoid possible numerical instabilities in the model. The Helmholtz filter solves the governing partial differential equation shown in Eq. 9:

$$\nabla(-R^2\nabla u) + u = D \quad (9)$$

Where: D is the input data; u is the filtered data; R is the filter radius, which in our model is set to 5.
The validation of the model results was carried out both qualitatively, by comparing time evolution of temperature and air speed in the ventilation cavity, and quantitatively, by means of the root mean square error (RMSE) and the normalized RMSE (NRMSE). The latter are indicators

of the accuracy of simulation results in comparison with measurement data. RMSE is defined as shown in Eq. 10, while NRMSE is calculated as in Eq. 11.

$$RMSE = \sqrt{\frac{1}{n}\sum_{i=1}^{n}(y_i - x_i)^2} \tag{10}$$

$$NRMSE = \frac{\sqrt{\frac{1}{n}\sum_{i=1}^{n}(y_i - x_i)^2}}{y_{\max} - y_{\min}} \tag{11}$$

Where: n is the sample size; y_i is the calculated data; x_i is the measured data; $y_{\max}$ and $y_{\min}$ are the maximum and minimum measured values.

A NRMSE value closer to 0 denotes a lower deviation between measured and simulated data.

Results and discussion

In this section, simulation results are compared to measurement data to validate the numerical model developed in COMSOL Multiphysics.

Figure 7 illustrates the comparison of simulated and measured temperature in position 1 (see Figure 2) at the south-facing bottom of the air cavity, during the winter day. A good agreement between the simulation results and the measurements data is shown, even if the former do not present the same time variation that characterize the latter. The numerical results follow relatively well the trend of the measurements, with a maximum deviation of ca. 1–2 °C, in the first part of the simulated period.

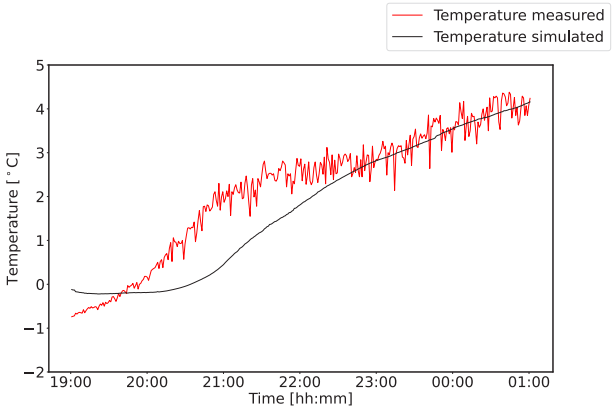

Figure 7: Comparison of simulated and measured temperature in position 1, in the winter day.

Figure 8 illustrates the comparison of simulated and measured air speed in position 1, during the winter day. In this case, the numerical results do present a certain time variation as the measured data, but their trend is constantly higher than that of the measurements. Therefore, the simulated values seem to follow relatively well the peaks of the measured values, but deviate of around 1–1.5 m/s from the lower measured values.

Figure 9 illustrates the comparison of simulated and measured temperature in position 6 at the north-facing bottom of the air cavity, during the winter day. The numerical results follow well the trend of the measurements only in a short part of the simulated period, with a consistent deviation of ca. 2 °C from the measured values in the rest of the simulated period.

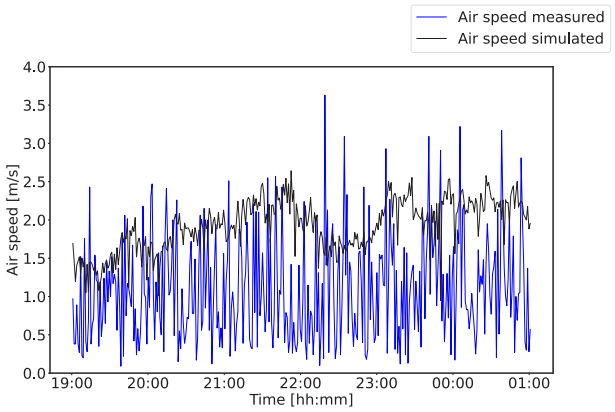

Figure 8: Comparison of simulated and measured air speed in position 1, in the winter day.

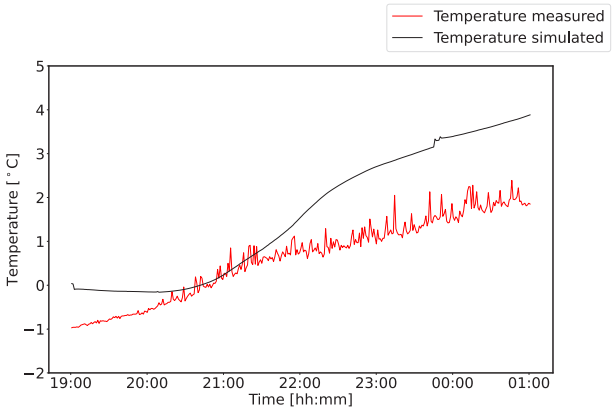

Figure 9: Comparison of simulated and measured temperature in position 6, in the winter day.

Figure 10 shows the comparison of simulated and measured air speed in position 6, during the winter day. The numerical results' trend is the same as in position 1 with the simulated values constantly deviating from the lower measured values.

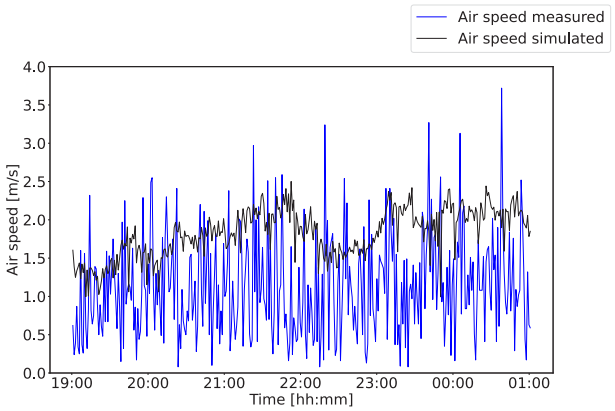

Figure 10: Comparison of simulated and measured air speed in position 6, in the winter day.

Figure 11 illustrates the comparison of simulated and measured temperature in position 1 at the south-facing

bottom of the air cavity, during the summer day. The numerical results present a certain time variation as the measured data and follow quite well their trend. However, the higher measured peaks, which go up to ca. 26–27 °C, are not reflected in the simulated values.

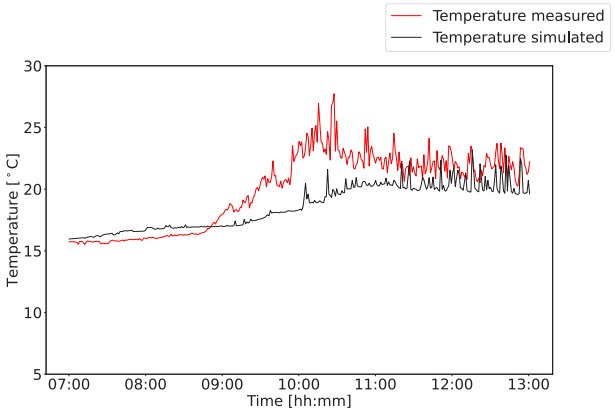

Figure 11: Comparison of simulated and measured temperature in position 1, in the summer day.

Figure 12 shows the comparison of simulated and measured air speed in position 1, during the summer day. The numerical results follow well the trend of the measurement data, especially in the second part of the period. However, the simulation curve deviates of around 0.2–0.4 m/s from the highest measured values throughout the period.

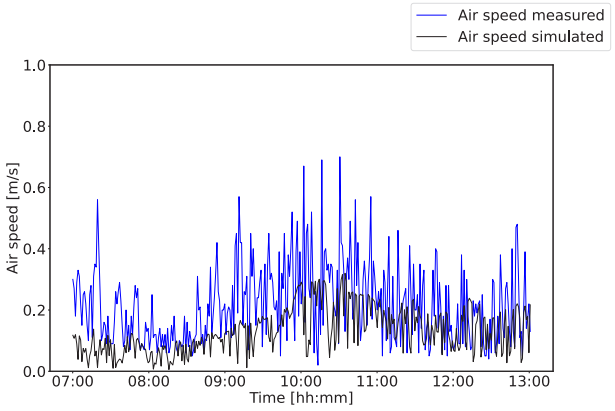

Figure 12: Comparison of simulated and measured air speed in position 1, in the summer day.

Figure 13 illustrates the comparison of simulated and measured temperature in position 6 at the north-facing bottom of the air cavity, during the summer day. The numerical results are in good agreement with the measured data, with lower deviation than in position 1.

Figure 14 shows the comparison of simulated and measured air speed in position 6 in the air cavity, during the summer day. The numerical results' trend is the same as in position 1, with a relatively good agreement with the measured data, especially in the second part of the period.

Tables 2 and 3 illustrate the results of RMSE and NRMSE for the simulated variables in all sensors positions, in both summer and winter days.

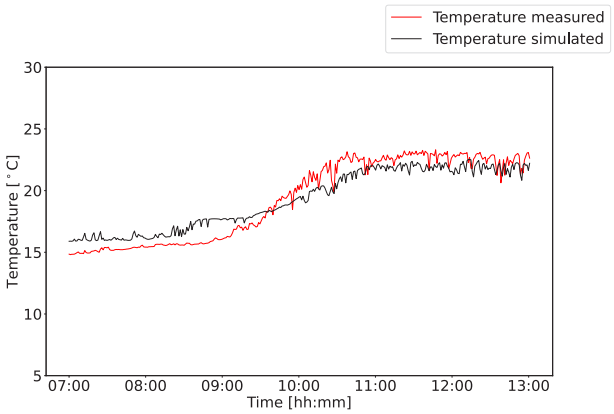

Figure 13: Comparison of simulated and measured temperature in position 6, in the summer day.

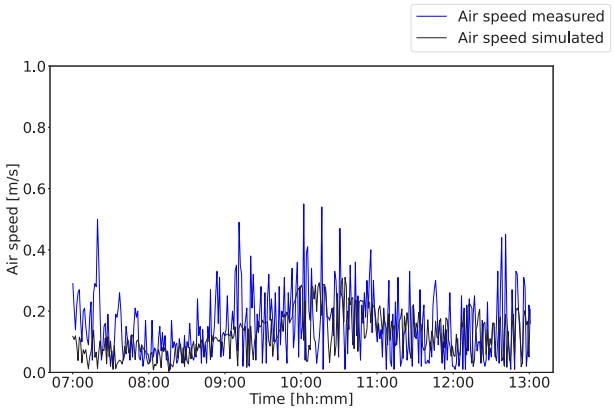

Figure 14: Comparison of simulated and measured air speed in position 6, in the summer day.

Table 2: RMSE results for the simulated variables.

	T1	T2	T3	T4	T5	T6	v1	v3	v4	v6
	°C						m/s			
Aug.31st	2.37	2.05	1.88	1.84	1,11	1.64	0.15	0.12	0.11	0.12
Dec.10th	0.73	0.62	0.83	0.86	1.19	1.17	1.11	1.17	1.14	0.99

Table 3: NRMSE results for the simulated variables.

	T1	T2	T3	T4	T5	T6	v1	v3	v4	v6
31st of August	0.19	0.14	0.13	0.16	0.16	0.19	0.22	0.20	0.24	0.23
10th of December	0.14	0.14	0.23	0.24	0.42	0.35	0.31	0.40	0.40	0.27

The RMSE and NRMSE values show a relatively good agreement between simulated and measured values during the summer day for both temperatures and air speed. A higher deviation is evident during the winter day, especially for the air speed values in sensor positions 3 and 4 at the top of the air cavity, and for the temperature in sensor positions 5 and 6 at the bottom of the air cavity.

The deviation between simulated and measured values might be related to several factors that can have affected the simulation results. First, the model in COMSOL Multiphysics did not include possible snow coverage during the simulated winter day, and the used solar radiation data from the weather station represented the global value, with no decomposition between direct and diffuse components. It is also worth noting that the modelled geometry is a simplification of the roof construction and does not reflect all possible real aspects; for instance, the roughness of the cavity surfaces was neglected, and the main parameters

for the modelled materials were assumed. Furthermore, the inlet and outlet pressures were given as a function of the C_P deduced from a similar case study and may differ for the specific roof analysed. The influence of the C_P values on the simulation results is especially significant in wind-driven ventilation conditions, as in the analysed winter day.

The results from this study could not be accurately compared with those from similar investigations due to the lack of comparable models in the literature. Furthermore, similar studies, as described in the introduction section, are based on different assumptions, e.g., air modelling as a laminar flow (Säwén et al. (2021)), or focus separately on the effect of thermal buoyancy (Villi et al. (2009) and wind Nore et al. (2010)).

Conclusion

This article presented the thermo-fluid dynamic model of the ventilated pitched roof of a full-scale experimental building in Trondheim (Norway). The modelling approach using COMSOL Multiphysics was explained and the results from transient simulations were presented. Specifically, simulations were performed for two periods within a summer day with low wind speed and high temperature/solar radiation, and a winter day with high wind speed and low temperature/solar radiation. Calculated temperature field and air flow speed along the cross section of the roof were compared to measurement data for validation. The simulation results show a good agreement with measurement data for both the air speed and the temperature in the air cavity, particularly in the summer day. However, some deviations between simulated and measured data were observed, most likely as a consequence of the assumptions and the simplifications adopted in the model.

The limitations of the study will be addressed by future research. First, the modelling approach will be further explored by testing different inputs, including boundary conditions and turbulence models. A parametric study on different inputs that might influence the simulation results will be performed, to define the sensitivity of the COMSOL model to different assumptions. Moreover, further investigation will be carried out to provide a better evaluation of the pressure coefficients (C_P) trend for the analysed building. For instance, on-site measurements of the C_P on the Test Cell roof will be performed. Similar ventilated roof constructions with available measurement data will be analysed with the same numerical approach, with the objective of further refining the model presented. Finally, the numerical model will be developed to include additional components on the roof, such as photovoltaic panels, and to analyse the influence that these components can have on the ventilation and temperature in the air cavity.

Acknowledgments

This article was written within a project that received a basic grant by the Research Council of Norway, which the authors gratefully acknowledge for the financial support.

References

COMSOL AB (2022). *COMSOL Multiphysics® v. 6.0*.

Blom, P. (2001). Venting of Attics and Pitched, Insulated Roofs. *Journal of Thermal Envelope and Building Science 25*(1), 32–50.

Bunkholt Schjøth, N., L. Gullbrekken, and T. Kvande (2020). Influence of Local Weather Conditions on Ventilation of a Pitched Wooden Roof. *Journal of Civil Engineering and Architecture 14*(1), 37–45.

Ciampi, M., F. Leccese, and G. Tuoni (2005). Energy analysis of ventilated and microventilated roofs. *Solar Energy 79*(2), 183–192.

Gagliano, A., F. Patania, F. Nocera, A. Ferlito, and A. Galesi (2012). Thermal performance of ventilated roofs during summer period. *Energy and Buildings 49*, 611–618.

Goia, F., C. Schlemminger, and A. Gustavsen (2017). The ZEB Test Cell Laboratory. A facility for characterization of building envelope systems under real outdoor conditions. *Energy Procedia 132*, 531–536.

Gullbrekken, L., T. Kvande, and B. Time (2017). Ventilated wooden roofs: Influence of local weather conditions - measurements. *Energy Procedia 132*, 777–782.

Gullbrekken, L., S. Uvsløkk, S. Geving, and T. Kvande (2018). Local loss coefficients inside air cavity of ventilated pitched roofs. *Journal of Building Physics 42*(3), 197–219.

Gullbrekken, L., S. Uvsløkk, T. Kvande, K. Pettersson, and B. Time (2018). Wind pressure coefficients for roof ventilation purposes. *Journal of Wind Engineering and Industrial Aerodynamics 175*, 144–152.

Lazarov, B. S. and O. Sigmund (2011). Filters in topology optimization based on Helmholtz-type differential equations. *International Journal for Numerical Methods in Engineering 86*(6), 765–781.

Lee, S., S. H. Park, M. S. Yeo, and K. W. Kim (2009). An experimental study on airflow in the cavity of a ventilated roof. *Building and Environment 44*(7), 1431–1439.

Li, D., Y. Zheng, C. Liu, H. Qi, and X. Liu (2016). Numerical analysis on thermal performance of naturally ventilated roofs with different influencing parameters. *Sustainable Cities and Society 22*, 86–93.

Nore, K., B. Blocken, and J. Thue (2010). On CFD simulation of wind-induced airflow in narrow ventilated facade cavities: Coupled and decoupled simulations and modelling limitations. *Building and Environment 45*(8), 1834–1846.

Nusser, B. and M. Teibinger (2013). Experimental investigations about the air flow in the ventilation layer of low pitched roofs. In *2nd Central European Symposium on Building Physics (CESBP 2013)*. Vienna (Austria), 9-11 September 2013.

Säwén, T., M. Stockhaus, C.-E. Hagentoft, N. Schjøth Bunkholt, and P. Wahlgren (2021). Model of thermal buoyancy in cavity-ventilated roof constructions. *Journal of Building Physics 45:4*, 413–431.

Tong, S. and H. Li (2014). An efficient model development and experimental study for the heat transfer in naturally ventilated inclined roofs. *Building and Environment 81*, 296–308.

Villi, G., W. Pasut, and M. D. Carli (2009). CFD modelling and thermal performance analysis of a wooden ventilated roof structure. *Building Simulation 2*(3), 215–228.

William, M. A., M. J. Suárez-López, S. Soutullo, and A. A. Hanafy (2021). Building envelopes toward energy-efficient buildings: A balanced multi-approach decision making. *International Journal of Energy Research 45*, 21096–21113.